Modified magnetomechancial model in the constant and low intensity magnetic field based on J–A theory*

Qingyou Liu(刘清友)[1,2], Xu Luo(罗旭)[1,†], Haiyan Zhu(朱海燕)[3], Jianxun Liu(刘建勋)[1], and Yiwei Han(韩一维)[1]

[1] College of Mechatronic Engineering of Southwest Petroleum University, Chengdu 610500, China
[2] Key Laboratory of Fluid and Power Machinery (Ministry of Education), Xihua University, Chengdu 600300, China
[3] College of Petroleum Engineering of Southwest Petroleum University, Chengdu 610500, China

(Received 12 December 2016; revised manuscript received 1 April 2017; published online 17 May 2017)

The existing magnetomechancial models cannot explain the different experimental phenomena when the ferromagnetic specimen is respectively subjected to tension and compression stress in the constant and low intensity magnetic field, especially in the compression case. To promote the development of magnetomechancial theory, the energy conservation equation, effective magnetic field equation, and anhysteretic magnetization equation of the original Jiles–Atherton (J–A) theory are elucidated and modified, an equation of the local equilibrium status is employed and the differential expression of the modified magnetomechancial model based on the modified J–A theory is established finally. The effect of stress and plastic deformation on the magnetic parameters is analyzed. An excellent agreement is achieved between the theoretic predictions by the present modified model and the previous experimental results. Comparing with the calculation results given by the existing models and experimental results, it is seen indeed that the modified magnetomechanical model can describe the different magnetization features during tension-release and compression-release processes much better, and is the only one which can accurately reflect the experimental observation that the magnetic induction intensity reverses to negative value with the increase of the compressive stress and applied field.

Keywords: modified Jiles–Atherton model, magnetomechanical effect, local equilibrium status

PACS: 75.80.+q, 62.20.f–, 75.30.Cr, 75.60.Ej **DOI:** 10.1088/1674-1056/26/7/077502

1. Introduction

Because of the combined action of geomagnetic field (about 40 A/m), stress–strain, and change in material microstructure, a self-spontaneous leakage magnetic field will be formed on the surface of the stress concentration or plastic deformation region in the ferromagnetic material. Based on this effect, the Russian researcher Dubov first proposed the concept of metal magnetic memory (MMM) in 1994,[1] and put forward the MMM technique in the 1998 fiftieth International Conference on welding.[2] As a new nondestructive detection method, which can effectively detect the early damage and assess the development trend of fatigue damage, it has been widely studied by the European and Chinese scholars.[3–7]

Essentially, the MMM effect is a result of the magnetomechanical effect, which is the change of magnetization resulting from the application of stress in the constant and low intensity field. Because of its complexity, lots of theoretical and experimental studies have been carried out.[8–11] Among them, Jiles and Atherton assumed that the main effect on the magnetization of the ferromagnetic material caused by cycling the applied stress is an irreversible change in the prevailing magnetization towards the anhysteretic magnetization $M_{\rm an}$, which is named the approach law, and the bulk magnetization M is the sum of a reversible component $M_{\rm rev}$ and an irreversible component $M_{\rm irr}$. Finally, they established the famous Jiles–Atherton (J–A) theory.[12–14] Then, based on the J–A theory, Sablik[11,15] and Jiles[16] took the elastic stress as an equivalent field H_σ and established the primal J–A–S model for the magnetomechanical effect, but the theoretical and experimental studies of them mainly focus on analyzing the magnetization due to a changed magnetic field under the constant stress or deformation, not the magnetization along with the changed stress in the constant magnetic field. In order to make the magnetomechanical model suitable for the magnetization along with the stress in the constant magnetic field, Sablik[17] employed two different relaxation constants $\zeta_{\rm a}$ and $\zeta_{\rm r}$ respectively for loading and releasing stress processes, and modified the approach law to improve the accuracy. Li *et al.*[18,19] applied the Rayleigh law to the stress, as well as a new linear stress-dependent term $\sigma \pm \eta E$ to improve the agreement near zero stress. During the stage of plastic deformation, Leng,[4] Wang,[5] Li,[6] Jiles,[20] Sablik,[21,22] Lo,[23] *et al.* analyzed the effect of plastic deformation and stress on the parameters, such as pinning constant k and coupling coefficient α, and derived different magnetomechanical models for plastic deformation.

*Project supported by the Major Program of Sichuan Province Science and Technology Plan, China (Grant No. 2015SZ0010) and the Scientific Research Foundation of Sichuan Province, China (Grant No. 2014GZ0121).

†Corresponding author. E-mail: 402585133@qq.com

© 2017 Chinese Physical Society and IOP Publishing Ltd

As for the approach law of the original J–A theory, the M_{an} is a global equilibrium status, it only happens when the magnetization is on the major hysteresis loop or initial magnetization curve. However, in the constant and low intensity field, the magnetization is on the minor hysteresis loop, and the application of stress induces change in magnetization toward the local equilibrium status M_o, so the approach law of M_{an} cannot be directly applied to model the magnetomechanical effect in the constant and low intensity field.[24–26] In order to solve this problem, Xu[27] established an equation of M_o and derived the J–A–F model at elastic deformation stage. Nevertheless, the calculated results of the J–A–F model are only in agreement with the experiment results during the tension-release process, and cannot reflect the experimental observation that the magnetic induction intensity B_e reverses to a negative value with the increase of the compressive stress and the external field. Additionally, there are also some mistakes in the existing models, such as having M_{an} confused with M.

The objective of this paper is to systematically identify and modify the inaccuracy of the energy conservation equation, effective magnetic field equation, and anhysteretic magnetization equation of the original J–A model and to develop a modified magnetomechanical model in the constant and low intensity magnetic field, which is suitable for both tension-release and compressive-release processes.

2. Modification of the J–A theory

The key parts of the J–A theory are the energy conservation equation, the effective magnetic field equation, and the anhysteretic magnetization equation. However, there are several queries about them by analyzing the classic papers introducing the J–A theory. So it is necessary to determine which expressions are reasonable.

2.1. The energy conservation equation

As is known, there are defects, irregularities of crystalline lattice defects, impurities, etc. within the ferromagnetic material, which hamper the movement of the domain wall, resulting in the hysteresis loss. According to the law of conservation of energy, the total magnetization energy is equal to the anhysteretic energy which would be in the ideal or unpinned case minus the hysteresis loss due to the pinning effect. By analyzing three different forms of energy conservation equation in the classic papers [11], [13], and [28], it is concluded that it is inaccurate to replace M_{irr} with M to calculate the hysteresis loss in Ref. [11], and unreasonable to regard the irreversible magnetization energy as the total magnetization energy in Ref. [13]. Additionally, Jiles added $(1-c)$ without a clear interpretation to the hysteresis loss, and there is also a mistake replacing B_e with H_e in Ref. [28]. Consequently, the correct expression of the energy conservation equation should be

$$\int M\,\mathrm{d}B_e = \int M_{an}\,\mathrm{d}B_e - \delta k \int \left(\frac{\mathrm{d}M_{irr}}{\mathrm{d}B_e}\right)\mathrm{d}B_e. \tag{1}$$

Differentiating Eq. (1) leads to

$$M = M_{an} - k\delta\frac{\mathrm{d}M_{irr}}{\mathrm{d}B_e} = M_{an} - \frac{k\delta}{\mu_0}\frac{\mathrm{d}M_{irr}}{\mathrm{d}H_e}. \tag{2}$$

2.2. The effective magnetic field H_e

The notion of effective magnetic field H_e plays a crucial role in the J–A theory, and the effect of the applied stress is represented by an equivalent field H_σ in the model of effective magnetic field H_e.[16] However, there is a discrepancy in the definition of the equivalent field H_σ among different authors: some of them claimed that the applied stress σ should be employed to calculate H_σ, such as Sablik in Ref. [11]; some of them assumed that the σ should be replaced with the residual stress σ_r, such as Leng in Ref. [4] and Sablik in Refs. [22] and [29]; and the others introduced the decomposition of H_σ into the magneto-elastic $H_{\sigma e}$ induced by elastic deformation and the magneto-plastic $H_{\sigma p}$ induced by plastic deformation, such as Wang in Ref. [5] and Li in Ref. [6]. Moreover, which one of M_{an} and M should be applied to H_e also remains a point of divergence.

Actually, depending on the situation, H_e should be discriminated between $H_{e(M_{an})}$ and $H_{e(M)}$, where $H_{e(M_{an})}$ is the anhysteretic effective magnetic field for anhysteretic calculating, and $H_{e(M)}$ is the hysteretic effective magnetic field for hysteretic calculating. So the H_e could be respectively written as

$$\begin{aligned} H_{e(M_{an})} &= H + \alpha M_{an} + H_{\sigma(M_{an})} \\ &= H + \alpha M_{an} + \frac{3\sigma}{\mu_0}\left[(r_{1(0)} + r'_{1(0)}\sigma)M_{an}\right. \\ &\quad \left. + 2(r_{2(0)} + r'_{2(0)}\sigma)M_{an}^3\right], \end{aligned} \tag{3}$$

$$\begin{aligned} H_{e(M)} &= H + \alpha M + H_{\sigma(M)} \\ &= H + \alpha M + \frac{3\sigma}{\mu_0}\left[(r_{1(0)} + r'_{1(0)}\sigma)M\right. \\ &\quad \left. + 2(r_{2(0)} + r'_{2(0)}\sigma)M^3\right]. \end{aligned} \tag{4}$$

2.3. The anhysteretic magnetization M_{an}

For the description of the anhysteretic magnetization, Jiles and Sablik have applied the modified Langevin function[15–20]

$$M_{an} = M_s\left[\coth\left(\frac{H_{e(M)}}{a}\right) - \frac{a}{H_{e(M)}}\right]. \tag{5}$$

Nevertheless, some researchers claimed that the anhysteretic magnetization should be given as an implicit of itself[21,22,30]

$$M_{an} = M_s\left[\coth\left(\frac{H_{e(M_{an})}}{a}\right) - \frac{a}{H_{e(M_{an})}}\right]. \tag{6}$$

According to the physical definition of M_{an}, it can be concluded that the curve of M_{an} along with the changed magnetic field H or stress σ should be a single value curve without hysteretic loop. It can be easily noticed that the assumption of the definition given by Eq. (5) leads to the conclusion that even the anhysteretic curve itself reveals hysteresis with respect to the stress σ, which is inconsistent with the physical definition of the hysteresis magnetization, as shown in Fig. 1(a). On the contrary, it is obvious that the calculated result of Eq. (6) is reasonable, as shown in Fig. 1(b), so equation (6) is the proper one.

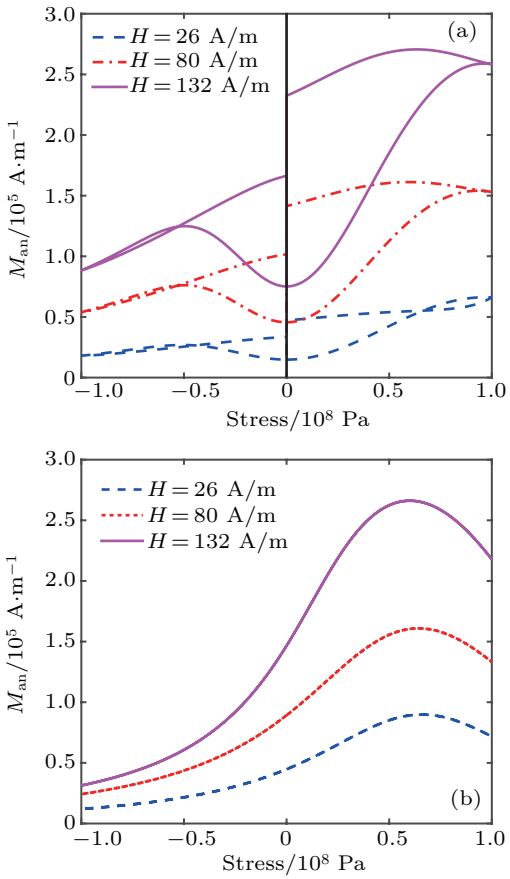


Fig. 1. (color online) Comparison between (a) Eq. (5) and (b) Eq. (6) for anhysteretic magnetization M_{an}.

3. Modification of the magnetomechanical model

3.1. The local equilibrium status M_o

The existing magnetomechanical models established by Sablik, Jiles, Leng *et al.* are all based on the global equilibrium status M_{an}. From the microcosmic perspective, the global equilibrium status M_{an} is the case of ideal crystal in which the domain walls move until they reach thermodynamic equilibrium without any pinning site obstruction. However, according to the results of the experiment, the application of stress in a constant and low intensity magnetic field induces change in magnetization toward a local equilibrium status M_o, which should be a stabilized loop around the anhysteretic magnetization curve, as shown in Fig. 2. So M_o can be taken as a middle status from M to M_{an}. In contrast with status M_{an}, M_o must have some pinning sites in the crystal structure of the material, and the pinning coefficient k_1 is employed to characterize the pinning loss from M_o to M_{an}. The smaller the k_1 is, the less the amount of pinning sites that cannot be overcome is, the closer the M_o is to M_{an}, indicating that the hysteresis loss is less from M_o to M_{an}.

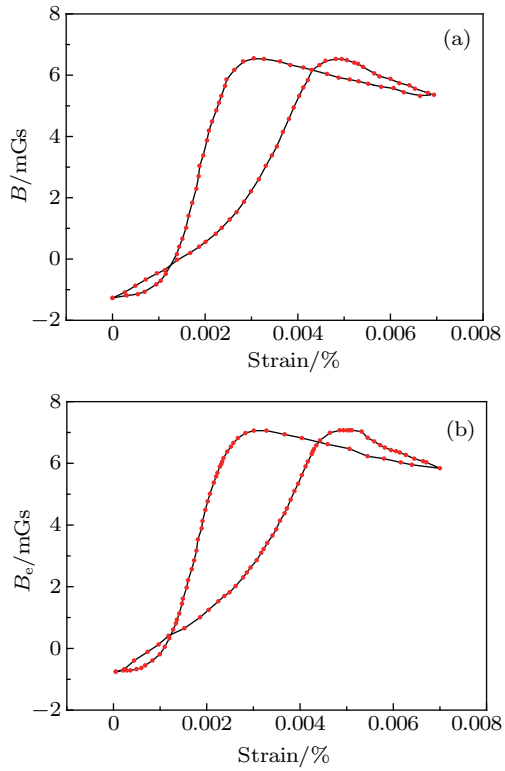


Fig. 2. (color online) The experimental hysteresis loops during different stress cycles in Figs. 4 and 5 of Ref. [31]: (a) cycles 500–505, (b) cycles 1600–1650.

Consider the energy balance from M_o to M_{an} [27]

$$\int M_o \,\mathrm{d}B_e = \int M_{an}\,\mathrm{d}B_e - \int \delta k_1 \,\mathrm{d}M_o + \int \frac{(M_{an}-M_o)\,\mathrm{d}W}{\eta}, \quad (7)$$

where $\int M_o \,\mathrm{d}B_e$ is the magnetization energy at the local equilibrium status, $\int \delta k_1 \,\mathrm{d}M_o$ is the hysteretic loss due to the pinning effect from M_o to M_{an}, k_1 is the pinning coefficient from M_o to M_{an}, which mathematically controls the amount of pinning sites that cannot be overcome by applying a stress in low magnetic field, $\int (M_{an}-M_o)/\eta \,\mathrm{d}W$ is the inelastic energy loss, η is the coefficient with the dimensions of the energy per unit volume, and W is the elastic energy per volume. Differentiating Eq. (7) leads to

$$M_o \,\mathrm{d}B_e = M_{an}\,\mathrm{d}B_e - \delta k_1 \,\mathrm{d}M_o + \frac{(M_{an}-M_o)\,\mathrm{d}W}{\eta}. \quad (8)$$

Because $B_e = \mu_0 H_e$, $W = \sigma^2/2Y$, replacing M_{an} with M_o in Eq. (3) and solving Eqs. (3) and (8) simultaneously give

$$\frac{\mathrm{d}M_\mathrm{o}}{\mathrm{d}\sigma}=\frac{\dfrac{1}{\delta k_1}(M_\mathrm{an}-M_\mathrm{o})\left\{3\left[\left(r_{1(0)}+2r'_{1(0)}\sigma\right)M_\mathrm{o}+2(r_{2(0)}+2r'_{2(0)}\sigma)M_\mathrm{o}^3\right]+\dfrac{1}{\eta}\dfrac{\sigma}{Y}\right\}}{1-\dfrac{\mu_0}{\delta k_1}(M_\mathrm{an}-M_\mathrm{o})\left\{\alpha+\dfrac{3\sigma}{\mu_0}\left[\left(r_{1(0)}+r'_{1(0)}\sigma\right)+6(r_{2(0)}+r'_{2(0)}\sigma)M_\mathrm{o}^2\right]\right\}}. \tag{9}$$

With the model parameters of Fig. 9 in Ref. [16], and by taking $k_1=1,2,5$, $\sigma=-100$ MPa to 100 MPa, the M_o variation with stress is shown in Fig. 3.

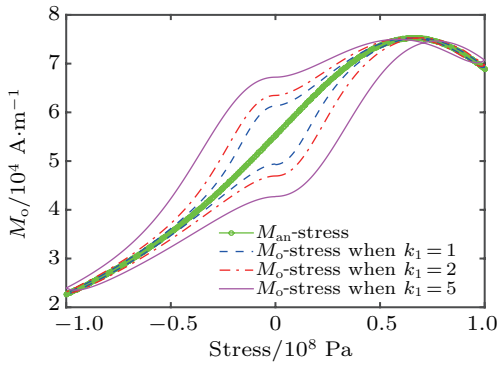


Fig. 3. (color online) The M_o–σ curves with different k_1 when $H=40$ A/m.

It can be seen that the curve of M_o–σ is a loop around the curve of M_an–σ. With the increase of k_1, the curve of M_o–σ is far away from the curve of M_an–σ, and the enclosed area increases, indicating a larger energy loss from M_o to M_an, which is nicely coincident with the theoretical predications above and the experimental results show that the magnetization caused by stress is moving towards a stabilized loop, as seen in Fig. 3.

3.2. The modification of magnetization M

According to the modified energy conservation equation in Subsection 2.1, by replacing the M_an with M_o in Eq. (3), the energy conservation equation from M to M_o is

$$\int M\,\mathrm{d}B_\mathrm{e}=\int M_\mathrm{o}\,\mathrm{d}B_\mathrm{e}-\delta k_2\int\left(\frac{\mathrm{d}M_\mathrm{irr}}{\mathrm{d}B_\mathrm{e}}\right)\mathrm{d}B_\mathrm{e}, \tag{10}$$

where k_2 is the pinning coefficient from M to M_o. Differentiating and ordering Eq. (10) give

$$\frac{\mathrm{d}M_\mathrm{irr}}{\mathrm{d}H_\mathrm{e}}=\frac{\mu_0}{k_2\delta}(M_\mathrm{o}-M). \tag{11}$$

Because $M=M_\mathrm{rev}+M_\mathrm{irr}$ and $M_\mathrm{rev}=c\,(M_\mathrm{o}-M_\mathrm{irr})$,

$$M=cM_\mathrm{o}+(1-c)M_\mathrm{irr}. \tag{12}$$

Differentiating Eq. (12) leads to

$$\frac{\mathrm{d}M_\mathrm{irr}}{\mathrm{d}\sigma}=\frac{1}{1-c}\left(\frac{\mathrm{d}M}{\mathrm{d}\sigma}-c\frac{\mathrm{d}M_\mathrm{o}}{\mathrm{d}\sigma}\right). \tag{13}$$

Differentiating Eq. (4) leads to

$$\begin{aligned}\frac{\mathrm{d}H_\mathrm{e}}{\mathrm{d}\sigma}=&\left\{\alpha+\frac{3\sigma}{\mu_0}\left[\left(r_{1(0)}+r'_{1(0)}\sigma\right)\right.\right.\\&\left.\left.+6(r_{2(0)}+r'_{2(0)}\sigma)M^2\right]\right\}\frac{\mathrm{d}M}{\mathrm{d}\sigma}\\&+\frac{3}{\mu_0}\left[\left(r_{1(0)}+2r'_{1(0)}\sigma\right)M\right.\\&\left.+2(r_{2(0)}+2r'_{2(0)}\sigma)M^3\right].\end{aligned} \tag{14}$$

The combination of Eqs. (11), (13), and (14) leads to the differential magnetization susceptibility

$$\frac{\mathrm{d}M}{\mathrm{d}\sigma}=\frac{-\dfrac{3}{k\delta}(M_\mathrm{o}-M)\left[\left(r_{1(0)}+2r'_{1(0)}\sigma\right)M+2\left(r_{2(0)}+2r'_{2(0)}\sigma\right)M^3\right]-\dfrac{c}{1-c}\dfrac{\mathrm{d}M_\mathrm{o}}{\mathrm{d}\sigma}}{\left\{\dfrac{\mu_0}{k\delta}(M_\mathrm{o}-M)\left\{\alpha+\dfrac{3\sigma}{\mu_0}\left[\left(r_{1(0)}+r'_{1(0)}\sigma\right)+6(r_{2(0)}+r'_{2(0)}\sigma)M^2\right]\right\}-\dfrac{1}{1-c}\right\}}. \tag{15}$$

Solving Eqs. (3), (4), (6), (9), and (15) simultaneously by using the standard variable-step Runge–Kutta method, the M changing with σ can be determined in the constant and low intensity field.

3.3. The interrelating effects of plastic deformation and stress on the model parameters

Figure 4 shows the stress against strain ($\varepsilon=\Delta L/L_0$).[21] It is seen that starting from zero applied stress, the deformation is increased linearly as the stress is increased. Once the yield stress σ_y is reached and the applied stress σ_f continues to increase, the deformation is increased nonlinearly from ε_y until some final deformation ε_f is reached. The deformation $\varepsilon_\mathrm{f}-\varepsilon_\mathrm{y}$ we shall call ε_p, the plastic deformation after yield. The difference $\sigma_\mathrm{f}-\sigma_\mathrm{y}$ is known as the strain hardening stress σ_F, which is the part of stress producing plastic deformation, resulting in the increase of dislocation density ζ_d. According to the experimental result of the x-ray test, the relationship between ζ_d and σ_F is[21]

$$\zeta_\mathrm{d}=\left[\left(\frac{|\sigma_\mathrm{F}|}{\alpha_k Gb}\right)+\zeta_{\mathrm{d}0}^{1/2}\right]^2, \tag{16}$$

where α_k is a constant which is given as 0.76, G is the specimen shear modulus as given by $G = Y/2(1+v)$, Y is the Yang's modulus, v is the Poisson's ratio, b is the appropriate Burgers vector magnitude for the specimen's dislocations, and ζ_{d0} is the initial dislocation density prior to plastic deformation.

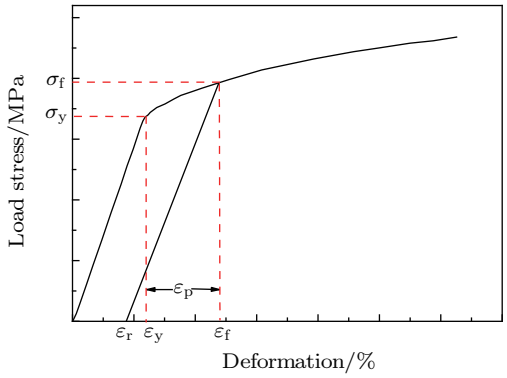


Fig. 4. (color online) Schematic diagram of tensile stress–strain curves for ferromagnetic materials. Applying a stress σ_f ($\sigma_f > \sigma_y$) to a specimen, the specimen deforms elastically and linearly up to yield stress σ_y, and then deforms plastically to strain ε_f, and the plastic deformation $\varepsilon_p = \varepsilon_f - \varepsilon_y$, in which ε_y is the strain at the yield point. After it is relaxed, the strain returns elastically to a residual strain ε_r.

With the change of stress and plastic deformation, the pinning coefficient k_2, scaling constant a and coupling coefficient α would be changed as follows:[6,21,23]

$$k_2 = k_\varepsilon + k'\sigma, \tag{17}$$

$$k_\varepsilon = \left[G_1 + \frac{G_2}{d}\right]\zeta_d^{1/2}k_0, \tag{18}$$

$$a = \left[G_3 + \frac{G_4}{d}\right]\zeta_d^{1/2}a_0, \tag{19}$$

$$\alpha = q_1 \ln\left(q_2\varepsilon_p + q_3\right), \tag{20}$$

where k_ε is the pinning coefficient related to dislocation, and will increase with the increase of plastic deformation, $k_0 = n\langle\varepsilon_\pi\rangle/2\mu_0 m$. $k' = -3/2m\lambda_s$, m is a constant, λ_s is the saturation magnetostriction constant, $k'\sigma$ indicates that the pinning effect will decrease with the increase of stress. a_0 is the initial scaling constant. d is the grain size. q_1, q_2, q_3 are the material constants.

4. The result of modification

Consider the model parameters of Fig. 9 in paper [16], and take $k_1 = 3$, $k_\varepsilon = k_0 = 2000$, $m = 0.2$, $\lambda_s = 1.5\times10^{-5}$, $\mu_0 = 4\pi\times10^{-7}$ N/A^2, $M_s = 1.71\times10^6$ A/m, $\alpha = 8.44\times10^{-6}$, $\eta = 605$, $\alpha_k = 0.76$, $r_{1(0)} = 2\times10^{-18}$ A^{-2}·m^2, $r'_{1(0)} = -1.5\times10^{-25}$ A^{-2}·m^2·Pa^{-1}, $r_{2(0)} = -2\times10^{-30}$ A^{-4}·m^4, $r'_{2(0)} = 5\times10^{-38}$ A^{-4}·m^4·Pa^{-1}, $c = 0.1$, $G_1 = G_3 = 0.81\times10^{-6}$ m, $G_2 = G_4 = 3.8\times10^{-12}$ m^2, $a_0 = 600$ A/m, $k_0/\mu_0 = 500$ A/m, $d = 1\times10^{-6}$ m, $C_{11} = 2.863\times10^{11}$ N/m^2, $C_{12} = 1.41\times10^{11}$ N/m^2, $q_1 = -2.15566\times10^{-4}$, $q_2 = 62.5447$, $q_3 = 0.0618315$. The magnetic induction B_e calculated by the modified model is shown in Fig. 5(e) when the external field is 26.4 A/m, 80 A/m, and 132 A/m.

Comparing with the results calculated by the existing models and the experimental results of No. 2 specimen in paper [32], we obtain the following results.

(i) According to the experimental results, the variation of B_e during the tension-release process is much more significant than that during the compression-release process, and the residual B_e after the tension-release process is much stronger than that after the compression-release process. The models established by Li and Xu and the modified model can describe the significant difference effectively, while Jiles' model cannot.

(ii) During the tension-release process, with the increase of the stress, the magnetic intensity B_e increases at first, then drops much slower for tension than for compression; the larger the external magnetic field H is, the more obvious the phenomenon is. It is at about 60 MPa that it reaches the maximum during tension. As shown in Fig. 5(c), it is at about 50 MPa where Li's model shifts into a reversal and the decaying rate of Li's model is much higher than that of the experimental result. In contrast, the results calculated by the Jiles, Xu, and the modified models can reflect this feature accurately.

(iii) During the compression-release process, the B_e firstly increases and then decreases along with the increase of the stress. When $H = 26.4$ A/m, the experimental values are all positive; while when $H = 80$ A/m and 132 A/m, parts of the testing data are lower than zero, and with the applied field H increasing, the experimental B_e decreases to negative. However, the theoretical predictions of magnetic intensity B_e by Jiles', Li's, and Xu's models are all positive, and the magnetic intensity B_e increases with the increase of the applied field H, which is contrary to the experimental phenomenon. In comparison, it can be seen that the theoretic predictions by the modified model are in considerably good agreement with the test data, particularly in the compressive situation, and the modified model is the only one which can describe the experimental phenomenon correctly.

(iv) Additionally, because the calculated result is very sensitive to the parameters,[24] the slope of the B_e–σ curve calculated by the modified model is much smaller in ascending and greater in descending than that of the experimental results when taking the same parameters of Fig. 9 in paper [16]. The problem can be solved by optimizing the related parameters. For example, the genetic algorithm (GA) is employed to optimize $r_{1(0)}$, $r'_{1(0)}$, $r_{2(0)}$, and $r'_{2(0)}$, and the objective function is defined as MSE $= \sum_i (X_i - x_i)^2/\sum_i x_i^2$, where X_i is the calculated B_e by the presented modified model, x_i is the experimental B_e, and i denotes the corresponding data point number. When $r_{1(0)} = 3.4\times10^{-18}$ A^{-2}·m^2,

$r'_{1(0)} = -1.5\times10^{-26}$ A^{-2}·m^2·Pa^{-1}, $r_{2(0)} = -15\times10^{-30}$ A^{-4}·m^4, $r'_{2(0)} = 5\times10^{-39}$ A^{-4}·m^4·Pa^{-1}, the MSE reaches its minimum, indicating that the calculated error between the calculated B_e and the experimental results is least, and the theoretic results are in better agreement with the experimental results, as shown in Fig. 5(f).

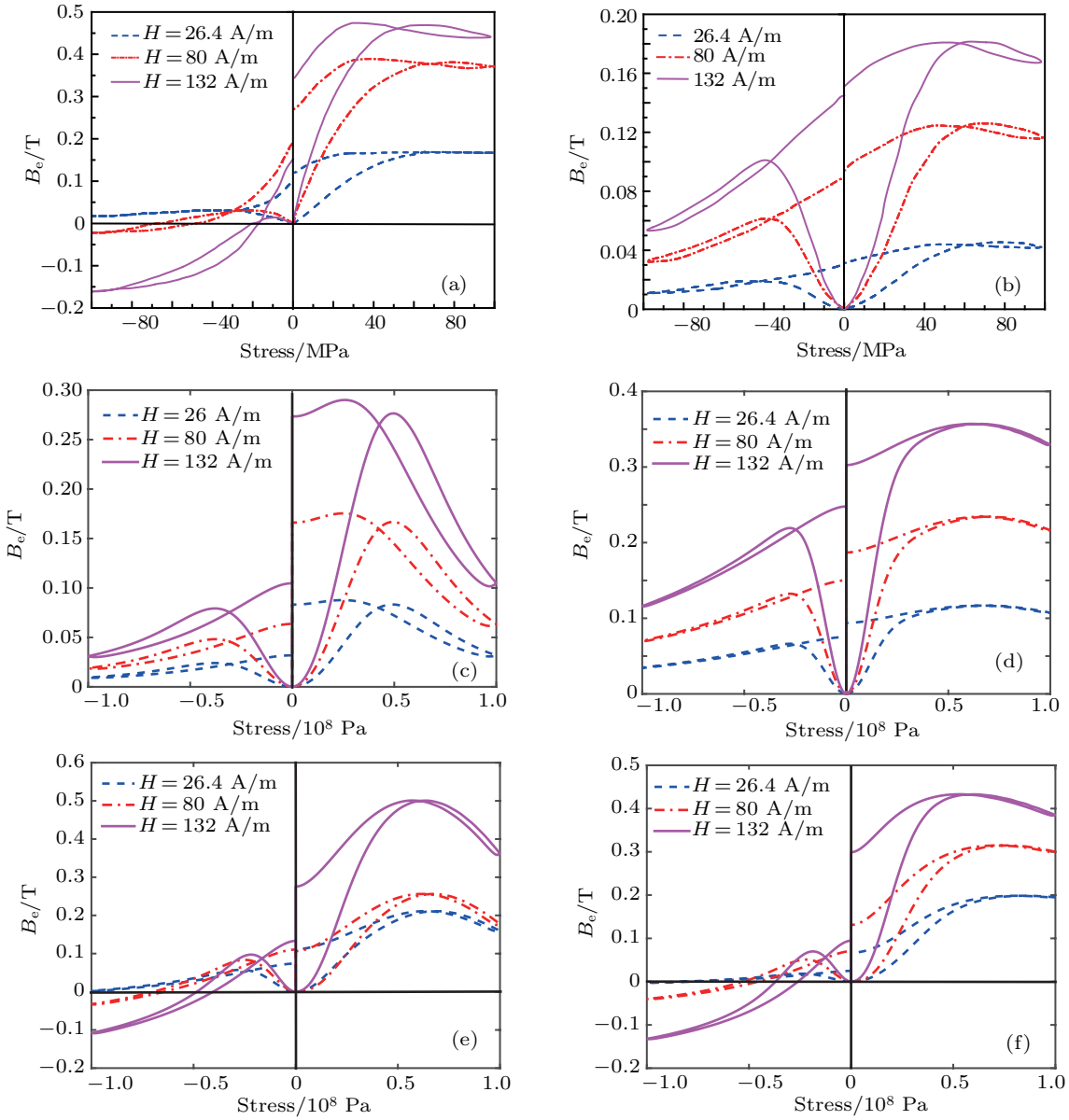


Fig. 5. (color online) Comparison of the different results given by the modified model, the original models, and the experiment. (a) The testing results of No. 2 specimen in paper [32]. (b) The results of Jiles' model in Fig. 9 of paper [16]. (c) The results of Li's model in paper [6]. (d) The results of Xu's model in paper [27]. (e) The result of the modified model. (f) The result of the modified model after optimizing parameters.

Based on the analysis above, it is concluded that the modified model can describe the experimental observation of the magnetomechanical effect in the constant and low intensity field much better than the existing models, and the modification is reasonable.

5. Conclusion

In this study, the simultaneous equations of the modified magnetomechanical model in the constant and low intensity field are established by modifying the J–A theory and employing the equation of M_o. Comparing with the results calculated by the existing models, the modified magnetomechanical model can describe the different magnetization features in tension-release and compression-release processes much better, and is the only one which can reflect the experimental observation that the magnetic induction intensity reverses to negative value with the increase of the external field and compressive stress effectively. Nevertheless, in order to make the modified model more accurate and effective, future work shall be aimed at optimizing the related parameters.

References

[1] http://www.energodiagnostika.com/article-about-mmm- method.html (last accessed Nov. 18, 2016)
[2] Dubov A A 1997 *Met. Sci. Heat. Treat.* **39** 401
[3] Dubov A A 2003 *Therm. Eng.* **50** 935
[4] Leng J, Liu Y, Zhou G and Gao Y 2013 *NDT & E Int.* **55** 42
[5] Wang Z D, Deng B and Yao K 2011 *J. Appl. Phys.* **109** 083928
[6] Li J W, Xu M Q, Leng J C and Xu M X 2012 *J. Appl. Phys.* **111** 063909
[7] Ahmad M I M, Arifin A, Abdullah S, Jusoh W Z W and Singh S S K 2015 *Steel Compos. Sruct.* **19** 1549
[8] Bozorth R M and Williams H J 1945 *Rev. Mod. Phys.* **17** 72
[9] Langman R 1985 *IEEE Tran. Magn.* **21** 1314
[10] Kwun H and Burkhardt G L 1987 *J. Appl. Phys.* **61** 1576
[11] Sablik M J, Kwun H, Burkhardt G L and Jiles D C 1987 *J. Appl. Phys.* **61** 3799
[12] Jiles D C and Atherton D L 1984 *J. Appl. Phys.* **55** 2115
[13] Jiles D C and Atherton D L 1986 *J. Magn. Magn. Mater.* **61** 48
[14] Jiles D C 1992 *IEEE Tran. Magn.* **28** 27
[15] Sablik M J, Rubin S W, Riley L A, Jiles D C, Kaminski D A and Biner S B 1993 *J. Appl. Phys.* **74** 480
[16] Jiles D C 1995 *J. Appl. Phys.* **28** 1537
[17] Sablik M J, Chen Y and Jiles D C 2000 *AIP Conf. Proc.* **509** 3037
[18] Li L and Jiles D C 2003 *J. Appl. Phys.* **93** 8480
[19] Li L and Jiles D C 2004 *J. Appl. Phys.* **95** 5934
[20] Jiles D C 2000 *J. Phys. D: Appl. Phys.* **21** 1196
[21] Sablik M J 2004 *IEEE Trans. Magn.* **40** 3219
[22] Sablik M J, Geerts W J, Smith K, Gregory A and Moore C 2010 *IEEE Trans. Magn.* **46** 491
[23] Lo C C H, Kinser E and Jiles D C 2003 *J. Appl. Phys.* **93** 6626
[24] Suliga M, Borowik L and Chwastek K 2015 *Arch. Metall. Mater.* **60** 409
[25] Atherton D L and Ton V 1990 *IEEE Trans. Magn.* **26** 1153
[26] Makar J M and Atherton D L 1995 *IEEE Trans. Magn.* **31** 2220
[27] Xu M X, Xu M Q and Li J W 2011 *NDT & E* **27** 1
[28] Jiles D C 1994 *J. Appl. Phys.* **76** 5849
[29] https://www.researchgate.net /publication/265264412 (last accessed Nov. 18, 2016)
[30] Chwastek K and Szczygłowski 2008 *Prz Elektrotechniczn* **84** 145
[31] Bao S, Jin W L, Huang M F and Bai Y 2010 *NDT & E Int.* **43** 706
[32] Craik D J and Wood M J 1970 *J. Phys. D: Appl. Phys.* **3** 1009